THE JOURNAL OF PHYSICAL CHEMISTRY B

ARTICLE

pubs.acs.org/JPCB

Dynamics of Structure Formation in a Discotic Liquid Crystal by Infrared Spectroscopy and Related Techniques

Periklis Papadopoulos,[‡,*] Christos Grigoriadis,[†] Nino Haase,[‡] Hans-Jurgen Butt,[‡] Klaus Müllen,[‡] and George Floudas[†,*]

[†]Department of Physics, University of Ioannina, 451 10 Ioannina, Greece and Foundation for Research and Technology-Hellas (FORTH-BRI)

[‡]Max-Planck Institute for Polymer Research, 55128 Mainz, Germany

Supporting Information

ABSTRACT:

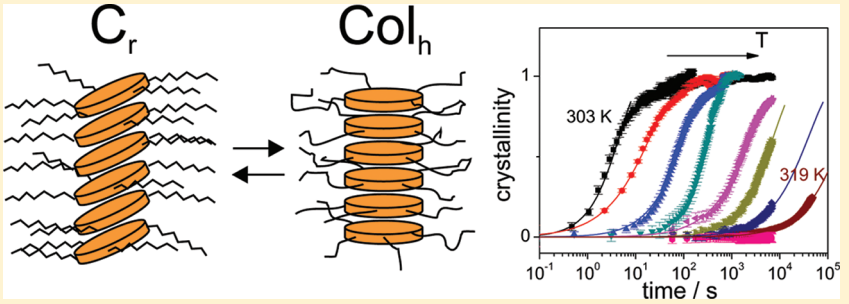

The dynamics of the herringbone structure formation have been studied in a monobromo hexa-*peri*-hexabenzocoronene derivative by infrared spectroscopy and complementary techniques. Selective probing of the vibration modes corresponding to the aromatic core and the alkyl chains, allowed investigation of their role in the phase transformation dynamics over an extraordinarily broad time-window ($1-10^5$ s). Identical kinetics were found suggesting that both the core and the alkyl chains simultaneously drive the system from the undercooled liquid crystalline to the crystalline phase with the herringbone structure.

1. INTRODUCTION

Discotic liquid crystals (DLC), consisting of rigid disk-shaped aromatic cores and disordered alkyl substituents self-assemble into columnar supramolecular structures.[1−3] Their self-assembly is driven by noncovalent intermolecular interactions favoring the π-stacking of aromatic cores and the unfavorable interactions between the cores and the alkyl chains leading to nanophase separation.[4−6] It was already pointed out by de Gennes,[7] that the incommensurability of flexible aliphatic side chains and rigid aromatic cores pose a packing problem in DLCs that could lead to a packing frustration with regions of high order interrupted by defects.

Recently the controlled synthesis of DLC bearing large aromatic cores, such as hexa-*peri*-hexabenzocoronenes (HBC), allowed extensive investigations of their self-assembly,[2−6,8] thermodynamics,[9−11] dynamics[8,12−16] and electronic[17,18] properties. Investigations with X-ray scattering revealed two main columnar structures in HBCs: a hexagonal liquid crystalline phase (Col_h) and a crystalline phase (C_r) at higher and lower temperatures, respectively. Of particular interest, with respect to the high charge carrier mobility along the columnar axis (i.e., molecular wires), is the crystalline phase composed of columns of tilted disks giving rise to the well-known *herringbone* structure. Recent efforts through the application of pressure[15,16,19] aided in constructing the complete phase diagrams for two dipole-substituted HBCs. According to these phase diagrams, the crystalline phase can be effectively stabilized at elevated pressures.

In parallel with the phase diagrams, there have been efforts[16,20] to probe the pathways of the phase transformation from the Col_h to the C_r phase in some HBCs. These experiments aimed at identifying the exact mechanism of phase transformation including metastable[20] or coexisting states, possible nucleation sites, and structural defects. Along these lines, a recent structural and dynamic investigation[21] in a monoiodo hexa-*peri*-hexabenzocoronene DLC revealed that the transformation is from a structurally weakly ordered but dipolarly well-ordered Col_h phase into a final C_r phase that is structurally well-ordered but dipolar disordered. The mechanism of phase transformation was shown to be nucleation and growth and the associated activation barriers were obtained from X-ray scattering, dielectric spectroscopy, and rheology. These activation barriers were found to be surprisingly low, which makes an investigation of the phase transformation kinetics feasible over an extended temperature range.

These studies, despite being instrumental in identifying the detailed pathways leading to the final crystalline phase, could not

Received: August 3, 2011
Revised: October 3, 2011
Published: November 03, 2011

Scheme I. Preparation of Br-HBC (i) 18 equiv. FeCl3, DCM, 1 h, 80%

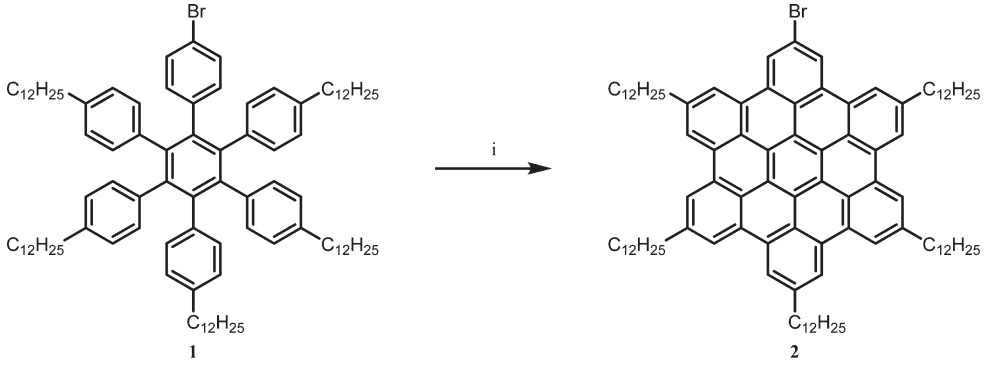

1 2

address the role of the alkyl chains in the self-assembly and phase transformation kinetics. The reason for this is that X-ray scattering patterns are dominated by the intra- and intermolecular packing of the cores, whereas dielectric spectroscopy is probing the kinetics through the dipole that, in these studies, was directly attached to the core. Rheology, despite being sensitive to the overall organization within the different phases, is lacking the pertinent molecular resolution. Addressing the role of alkyl chains on the packing within the different phases and, more importantly, on the kinetics of phase transformation requires molecular resolution and separate but simultaneous probing of the alkyl chains and the aromatic cores. Earlier studies by means of infrared spectroscopy[22] as well as by molecular simulations[23] already suggested that the alkyl chains possess structural disorder within the Col_h and C_r phases.

Here, we address the role of alkyl chains on the organization and phase transformation to the herringbone structure. Therefore, infrared spectroscopy (IR) and complementary techniques (dielectric spectroscopy, rheology) were employed to study a monobromo hexa-*peri*-hexabenzocoronene derivative. IR is a very sensitive probe of both the alkyl chain and core dynamics. These concerted efforts allowed probing the transformation kinetics over an extraordinarily broad time-window, ranging from seconds to days. We show that both the alkyl chains and the aromatic core are simultaneously involved in the phase transformation.

2. EXPERIMENTAL SECTION

2.1. Synthesis. The synthesis of the monobromo hexa-*peri*-hexabenzocoronene (HBC) has been reported earlier.[19] After preparing the 1-(4-bromo)-2,3,4,5,6-pentakis-(4-dodecylphenyl) hexa-phenylbenzene **1** (Br-HPB) via a Diels–Alder cycloaddition, the desired Br-HBC-derivative can be subsequently obtained through an intramolecular Scholl reaction in good yields (80%). The molecular structure is shown in Scheme I.

2.2. Differential Scanning Calorimetry (DSC). The thermal behavior of the HBC-Br was determined by differential scanning calorimetry (DSC) on cooling and subsequent heating with different rates (10, 5, and 2 K/min) with a Mettler 30 DSC.

2.3. X-ray Scattering. The 2D wide-angle X-ray scattering (WAXS) experiments were performed by using the X-ray beam with pinhole collimation and a two-dimensional detector (Siemens A102647) with 1024 × 1024 pixels. A double graphite monochromator for the CuKα radiation (λ = 0.154 nm) was used. Measurements in the range from 223 to 413 K were made from macroscopically oriented cylindrical filaments with a diameter of 0.7 mm prepared with a microextruder at 298 K. All patterns were recorded with a near vertical orientation of the filament axis and the X-ray beam perpendicular to the filament.

2.4. Pressure-Volume-Temperature (PVT) Measurements. The PVT measurements on the HBC-Br sample were made with a Gnomix dilatometer using the confining fluid technique (mercury). Measurements were made under "isobaric" conditions within the temperature range from 313 to 433 K and for pressures in the range from 10 to 200 MPa following a heating/cooling protocol (Supporting Information).

2.5. Infrared Spectroscopy. Infrared absorption spectra were measured with an FTS 6000 FTIR spectrometer equipped with a UMA 500 microscope. A photovoltaic MCT detector was used (KMPV50, Kolmar Technologies), allowing for best linearity, even at high absorbance values. The sample was pressed between two germanium windows and formed a film with a thickness of about 10 μm. The spectral resolution was 2 cm^{-1}. A Linkam THMS600 heating stage with a TMS91 controller and ZnSe windows was employed for the temperature dependent studies in the range 293–363 K. The quasi-static measurements were performed using an average rate of 1 K/min. The kinetics of the structure formation were studied at fixed temperatures using temperature jumps, from the molten state (T = 363 K) to different temperatures in the range 293–321 K, with a cooling rate of 50 K/min. The time resolution was 0.5 s.

2.6. Dielectric Spectroscopy. Dielectric measurements were made under (i) "isobaric" conditions as a function of frequency for different temperatures and (ii) under "isobaric/isothermal" conditions following temperature jumps from the same initial temperature (373 K) to different final temperatures within the range 308–321 K. The measurements for (i) were performed at atmospheric pressure, and for frequencies in the range from 10^{-2} to 10^{6} Hz. For the kinetic experiments, successive spectra of 10 min long were recorded and the lowest frequency was set to 0.1 Hz that provides a compromise between the time-scale of the process and the time needed for a spectrum to be recorded. In general, the complex dielectric permittivity $\varepsilon^* = \varepsilon' - i\varepsilon''$, where ε' is the real and ε'' is the imaginary part, was obtained as a function of frequency ω, temperature T, (or pressure P) and time, i.e., $\varepsilon^*(T,\omega,t)$.[24,25] The analysis of the time-dependent spectra was made using the empirical equation of Havriliak and Negami (HN):

$$\varepsilon^*(T,\omega,t) = \varepsilon_\infty(T,t) + \frac{\Delta\varepsilon(T,t)}{[1 + (i\omega\tau_{HN}(T,t))^{\alpha(t)}]^{\gamma(t)}} + \frac{\sigma_0(T,t)}{i\varepsilon_f\omega} \quad (1)$$

Where $\varepsilon_\infty(T,t)$ is the high frequency permittivity, $\tau_{HN}(T,t)$ is the characteristic relaxation time in this equation, $\Delta\varepsilon(T,t) = \varepsilon_o(T,t) - \varepsilon_\infty(T,t)$ is the relaxation strength, α, γ (with limits $0 < \alpha, \alpha\gamma \leq 1$) describe, respectively, the symmetrical and asymmetrical broadening of the distribution of relaxation times, σ_o is the dc-conductivity, and ε_f is the permittivity of free space.

2.7. Rheology. An advanced rheometric expansion system (ARES) equipped with a force-rebalanced transducer was used in the oscillatory mode for recording the viscoelastic properties of the HBC-Br. Depending on the temperature range, two transducers were used with 2000, 2 g·cm and 200, 0.2 g·cm upper and lower sensitivity, respectively. The sample was prepared on the lower plate of the 10 mm diameter parallel plate geometry setup and heated under a nitrogen atmosphere until it could flow. Subsequently, the upper plate was brought into contact, the gap thickness was adjusted to 1 mm, and the sample was slowly cooled to the desired starting temperature. For the lower temperatures investigated (near the glass temperature) plates with 6 mm diameter were employed. The storage (G') and loss (G'') shear moduli were monitored in different types of experiments. First, the linear and nonlinear viscoelastic ranges were identified, by recording the strain amplitude dependence of the complex shear modulus $|G^*|$ at selected temperatures. In the subsequent experiments, strain amplitudes within the linear viscoelastic range were used. These experiments involved (i) isochronal (ω = 10 rad/s) temperature sweeps with a rate of 2 K/min and (ii) temperature jumps from the same initial temperature (373 K) corresponding to the liquid crystalline phase to different temperatures in the range 315−320 K corresponding to the crystalline phase.

3. RESULTS AND DISCUSSION

3.1. Probing the Equilibrium Phases. Results for the specific heat, C_P, specific volume, V, and shear modulus, $|G^*|$, are depicted in Figure 1. In addition, the figure provides some representative 2D WAXS images at two temperatures corresponding to the crystalline (C_r) phase at 223 K and to the columnar hexagonal liquid crystalline phase (Col_h) at 413 K. Within the Col_h phase, the 2D WAXS images display a set of strong meridional reflections associated with the typical intracolumnar periodicity of graphite (of 0.35 nm) and a set of equatorial reflections with ratios $1:3^{1/2}:4^{1/2}$ relative to the primary peak that correspond to the (10), (11), and (20) reflections of a hexagonal lattice. Four additional reflections are evident in the 2D WAXS image with equivalent Bragg spacing of $d \approx 0.5$ nm. These reflections appear at azimuthal angles of ∼90° (see Supporting Information) and are evident only in HBCs bearing dipolar groups thus reflecting dipole−dipole correlations.[19,21] The C_r phase is characterized by a set of strong equatorial reflections that correspond to the (10), (01), (20), (11), and (21) reflections of a monoclinic unit cell with representative lattice parameters a = 2.42 nm, b = 1.81 nm and γ = 80° for HBC-Br, (obtained at 223 K by cooling from the high temperature phase). The off-meridional reflections originate from a tilt of the discotic cores with respect to the columnar axis, which is the characteristic of the *herringbone* structure identified earlier by NMR[6] and WAXS.[5]

The thermodynamics of the C_r to Col_h transformation investigated with DSC revealed a first order transition (Figure 1, top) at 340 K (on heating) with a heat of fusion of 36 J/g. PVT measurements on the same sample, show a discontinuous increase

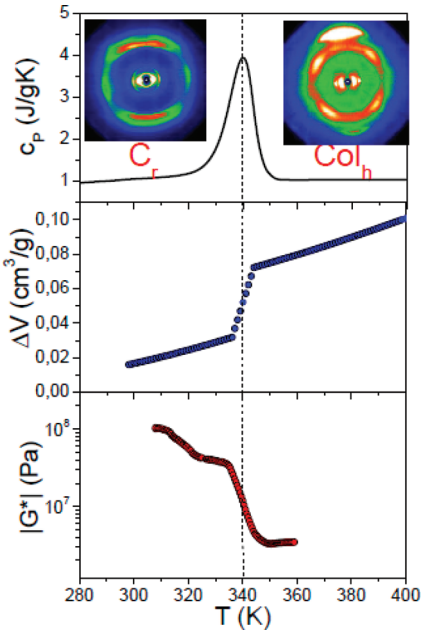

Figure 1. A composite plot showing the heat capacity c_P (top), the change in specific volume, ΔV (middle) and the shear modulus, $|G^*|$ (bottom) (ω = 10 rad/s), obtained on heating from differential scanning calorimetry, pressure-volume-temperature, and rheology, respectively. The heating rates were 10, 1, and 2 K/min in DSC, PVT, and rheology, respectively. The vertical line separates the low temperature C_r phase from the Col_h phase at higher temperatures. The insets are 2D-WAXS images taken at 223 and 413 K, which correspond, respectively, to the C_r and Col_h phases.

of the specific volume at approximately the same temperature (Figure 1, middle). In addition, the two phases possess distinctly different viscoelastic properties (Figure 1 bottom), as shown by the precipitous decrease of the complex modulus $|G^*|$ during the "isochronal" heating at a frequency of 10 rad/s. Lastly, small differences in the transition temperature are due to the different heating rates in the different experiments.

Infrared absorption spectra in the C_r and Col_h phases are shown in Figure 2. In particular, the spectral regions 1480−1430, 1370−1300, and 750−710 cm^{-1} are known to be sensitive to alkyl chain conformation.[26−28] They are based on comparisons with alkanes,[26,27,29] polyethylene,[30,31] as well as from an earlier study on alkyl-decorated HBC.[22] Identification of the remaining modes are based on IR databases and comparison with hexa-benzo-coronenes (HBC) and are summarized in Table 1.[25−33] The double bands for HBCs reflect the different symmetry of vibrations (symmetric vs antisymmetric).

In general, IR absorption spectra show noticeable changes with temperature and in particular band shifts and intensity changes. These effects can be attributed to (a) thermal expansion, in combination with bond potential anharmonicity, (b) conformational changes, and (c) phase transitions. The former leads to a negative shift of the vibrational frequency, in agreement with previous studies.[36] The other two may lead to positive or negative shifts, depending on the changes in packing. Among the different contributions, the one from the phase transitions is usually the most prominent. The Grüneisen parameter that relates the volume to the changes in the vibration frequency can also be extracted from the thermodynamic data (see Supporting Information). However, its macroscopic value is significantly lower than unit, suggesting

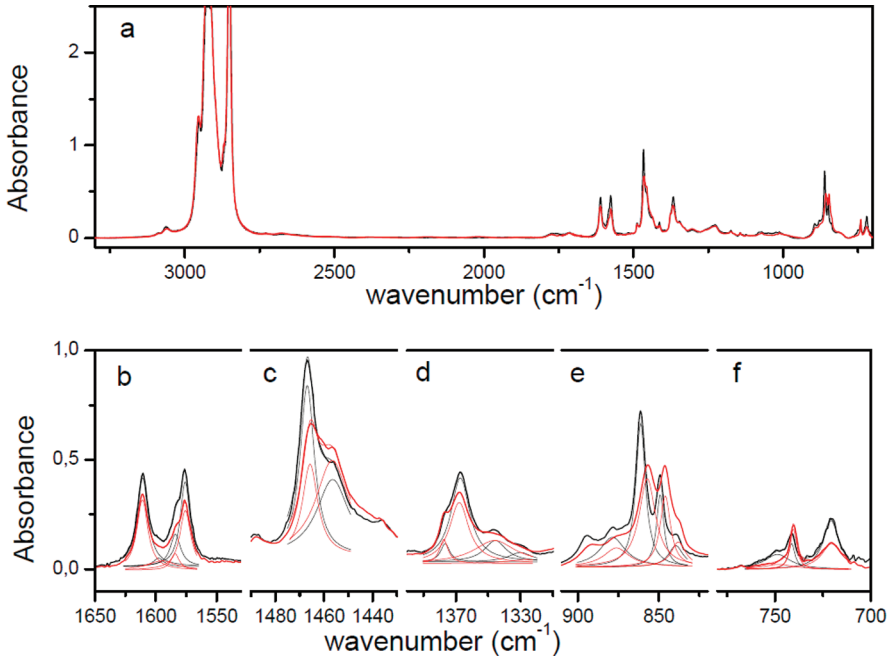

Figure 2. (a) Absorption IR spectra of HBC-Br in the C_r (T = 303 K, black curve) and Col_h phase (T = 363 K, red curve) and (b)−(f) details of the absorption spectra at regions that are sensitive to the conformational changes. The assignments are summarized in Table 1. The curves are fitted with a sum of Lorentz functions (dotted lines) with varying center, width, and area.

Table 1. Summary of the Most Important Absorption Bands (Figure 2)[a]

wavenumber (cm^{-1})	assignment	comments
3063	C−H stretching	aromatic hydrogens of HBC[32]
1611	C═C stretching	outer parts of HBC disk[32]
1576	C═C stretching	outer parts of HBC disk[32]
1467	CH_2 deformation	trans alkyl segments[22,30]
1459	CH_2 deformation	gauche alkyl segments[22,32]
1377	CH_3 deformation	C_{12} chain ends[22,28]
1367	core, CH_2 wagging	kinks, gtg defects in C_{12} chains[22,28]
1346	core, CH_2 wagging	gauche gg defects in C_{12} chains[22,28]
1340	CH_2 wagging	end gauche in C_{12} chains[22,28]
1300	CH_2 wagging	gtg' defects in C_{12} chains[22,28]
861	C−H out-of-plane bending	aromatic hydrogens of HBC[22,32,33]
849	C−H out-of-plane bending	aromatic hydrogens of HBC[22,32,33]
~750	CH_2 rocking	C_{12} chains, alternating trans−gauche[34]
742	CH_2 rocking	C_{12} chains[31]
720	CH_2 rocking	C_{12} trans segments[31]

[a] The assignments of the C_{12} chain vibrations are based on comparison with polyethylene and related systems.

that the anisotropic molecular properties should be considered instead. In Figure 2, the IR spectra of HBC-Br taken at 303 K (C_r) and 363 K (Col_h) are compared. The most prominent differences are observed in bands corresponding to the alkyl side chains and to the aromatic hydrogens (Figure 2b−f), as a result of the different packing motifs that affect the vibrational modes. These modes can be employed as a fingerprint of the phase state and thus facilitate, for the first time, a study of the phase transformation dynamics in going from the high temperature Col_h phase to the C_r phase at lower temperatures by separate probing of the side chains and of the aromatic core. In addition, all vibration peaks show an increasing broadening on heating. This broadening can be attributed to the distribution of molecular environment as well as the excited state lifetime. Therefore, a minimum value for the lifetime can be extracted from the fwhm bandwidth obtained by band deconvolution with Lorentzian profiles (Figure 2). As an example, the lifetime for the C−H out-of-plane bending mode changes from 4.8 (at 303 K) to 2.9 ps (at 363 K), whereas for the C═C stretching the change is only from 3.7 to 3.3 ps at the same temperatures. These estimated lifetimes are, as expected, some orders of magnitude shorter than the rotational motion of the disks about the columnar axis (disk axial motion).[12−16] Therefore, from IR spectra one can extract information about the instantaneous system conformation rather than dynamics.

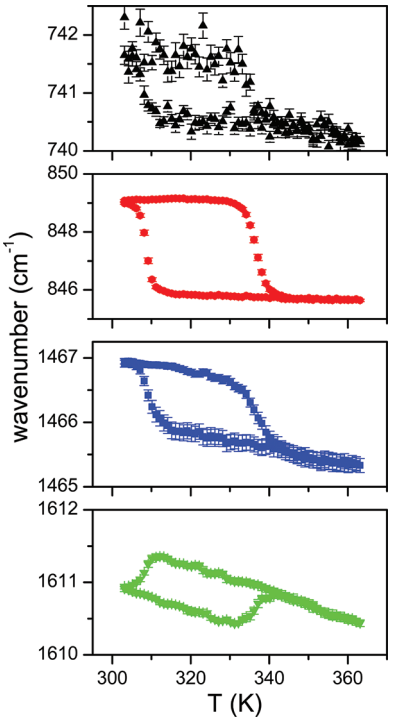

Figure 3. Temperature dependence (heating and cooling runs) of the frequency of four different vibrations: CH_2 rocking (black up triangles), C−H out-of-plane bending (red circles), CH_2 deformation (blue squares), and C═C stretching (green down triangles).

The temperature dependence of the characteristic frequency of four different vibrations corresponding to the CH_2 rocking, CH_2 deformation, C−H out-of-plane bending, and C═C stretching is shown in Figure 3. In general, vibration frequencies decrease with temperature when the system remains in one phase, due to thermal expansion. All modes give a clear signature of the phase transformation with a large hysteresis, but undoubtedly, it is the C−H out-of-plane bending mode that gives a better signature of the phase transformation. The first three show a negative step during the C_r to Col_h phase transformation, which is the expected trend due to thermal expansion. In contrast, the C═C vibration shows the opposite trend and shift to higher frequencies. Since this is an in-plane vibration, this shift reflects the stronger π-orbital overlap of the HBC discs in the Col_h phase. Indeed, previous detailed X-ray studies on the similar monoiodo hexa-*peri*-hexabenzocoronene (HBC-I) showed that the distance between the discs decreases from about 0.40 nm in the C_r phase to 0.35 nm in the Col_h.[11]

To estimate the volume fraction, ϕ, of the final C_r phase, a given spectrum is fitted with a sum of reference curves, corresponding to the liquid crystal and crystalline phases at a certain temperature. For the selection of the reference spectra corresponding to the two pure phases, the results of the X-ray study (Figure 1) were used as a guide. This ensures that the selected reference spectra, taken at 303 and 363 K, respectively, correspond to the C_r and Col_h phases. Following this approach, $\phi(T)$ can be determined by fitting each measured spectrum with the following equation:

$$A(T) = \phi(T)A_c + (1 - \phi(T))A_a \qquad (2)$$

where $A(T)$ is the measured absorption spectrum at temperature T, A_c is the profile of the reference C_r state, and A_a the reference

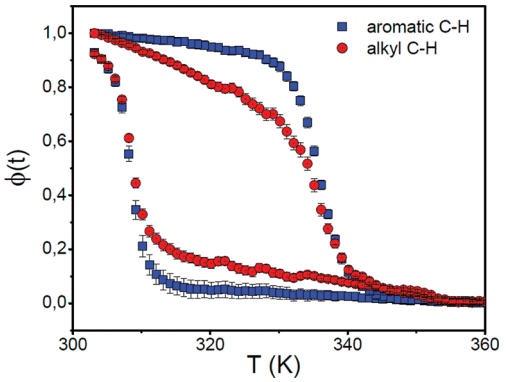

Figure 4. Temperature dependence of the volume fraction of the C_r phase obtained from the deconvolution of aromatic C−H (Figure 2e, squares) and alkyl (Figure 2c, circles) absorption bands. The latter show a systematic bias toward 0.5 due to the large temperature dependence of the respective vibrations. The reference spectra (see eq 2) were measured at 363 K (Col_h) and 303 K (C_r).

Col_h phase. The whole spectrum in the ranges shown in Figure 2c,e was fitted with eq 2 in order to obtain $\phi(T)$. Ideally, the IR spectra of the C_r and Col_h phases should be measured at the same temperature as the spectrum to be analyzed; however, this is not possible in the quasi-static case. As an approximation, we select the highest and lowest temperatures where C_r and Col_h phases are stable, respectively, that is 303 and 363 K.

Figure 4 provides the results of the above analyses with respect to ϕ for the aromatic and alkyl C−H vibration modes during a heating−cooling run (rate of 1 K/min). The results for both vibrations are qualitatively similar, however, even though the transition temperatures are in good agreement, the volume fraction of the C_r phase obtained by the CH_2 deformation band, is biased toward 0.5. This is an indication that the spectral profiles of each phase are temperature dependent, reflecting conformational changes in the alkyl chains taking place within the C_r phase, even though the aromatic cores are fixed to the herringbone structure. The latter is in agreement with earlier heteronuclear solid state NMR investigations of the dynamic order parameter corresponding to the C−H bonds in the core and on the alkyl chains within the C_r phase of various HBC derivatives.[16]

In order to obtain quantitative information about different parts of the molecule, in particular the core and alkyl chains, the spectral ranges of Figure 2b−f were fitted with a sum of Lorentz functions. A straight baseline was subtracted in all cases. Quantitative information about the conformation of alkyl chains can be obtained from the bending vibrations in the region 1480−1430 cm^{-1} (Figure 2c), because the 1370−1300 cm^{-1} overlaps with core vibrations.[22] It should be noted that the absorption bands of alkyl chains differ considerably from semicrystalline polyethylene,[31,35] with the characteristic sharp doublets of HBC-Br at ~1470, 1460, and 740, 720 cm^{-1} not showing up in the former. Since splitting in crystals arises from the dense packing and the coupling between vibrators, this indicates that alkyl chains in HBC-Br possess different packing motifs as compared to the alkyl chains in PE. In addition, the C_r phase of HBC-Br is different from the low temperature crystalline phase of HBC decorated solely with dodecyl chains, where the infrared spectra were similar to crystalline alkanes.[22] Therefore, an analysis similar to the grafted chains is more feasible.[27] The high (1467 cm^{-1}) and low frequency (1459 cm^{-1}) CH_2 bending vibrations are assigned to trans and

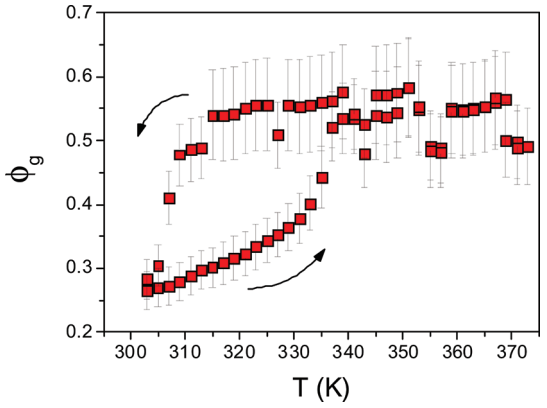

Figure 5. Fraction of gauche conformers in the alkyl chains as a function of temperature. The ratio of intensities of the band at 1459 cm^{-1} to the total CH_2 deformation intensity (including the 1467 cm^{-1} band), is a measure of gauche conformers and disorder of alkyl chains.

gauche segments, respectively. From the integrated absorbance the gauche fraction is estimated as, $\phi_g = (I_{1459})/(I_{1467} + I_{1459})$, and the results are shown in Figure 5. Depending on the deconvolution, the lower frequency components (~1440 cm^{-1}) may cause small variations in the calculated values, indicated by the error bars. There is a pronounced similarity in the temperature dependence of ϕ_g (Figure 5) with that of the volume fraction of the crystalline phase (Figure 4). Within the Col_h phase, the 2/3 of the conformations are gauche. On decreasing the temperature, at about 310 K, they change abruptly in favor of the extended trans conformations within the C_r phase. Despite this, roughly 1/3 of the conformations are still gauche. On subsequent heating, the alkyl chains undergo continuous conformational changes favoring the gauche state and at ~335 K, they reach their 2/3 fraction, characterizing the final Col_h phase. These results demonstrate that the alkyl chain conformations can also be used as fingerprints of the phase transformation.

This brings up the question whether these changing conformations of the alkyl chains are the driving force for the formation of the crystalline phase. We recall here the incommensurability problem between the flexible aliphatic side chains and the rigid aromatic cores that can result in a packing frustration. A way to address this question is by following the kinetics of phase transformation by separate probing of the aromatic and alkyl vibrations. A faster time-scale of organization for the latter (i.e., alkyls first) would imply that, indeed, the formation of the herringbone structure is driven by the packing of the alkyl chains. However, a single time-scale would imply that the packing of both of the aromatic cores and of the alkyl chains need to be considered. Lastly, a slower time scale for the alkyl chains (i.e., cores first) would suggest that the rate-determining step for the formation of the crystalline phase is the tilting of the aromatic cores. Such a distinction is possible provided that the dynamics differ by at least 10 s (at the lowest temperature investigated).

3.2. Kinetics of Phase Transformation. The kinetics of the C_r phase formation was investigated following temperature jumps from an initial temperature corresponding to the Col_h phase. We first describe the IR kinetics followed by DS and rheology results. As discussed earlier, the most unambiguous method of obtaining the volume fraction of the C_r phase is by fitting the C−H out-of-plane deformation spectral range (Figure 2e) with eq 2. For comparison, the CH_2 deformation bands from the alkyl chains (Figure 2c) are also shown in

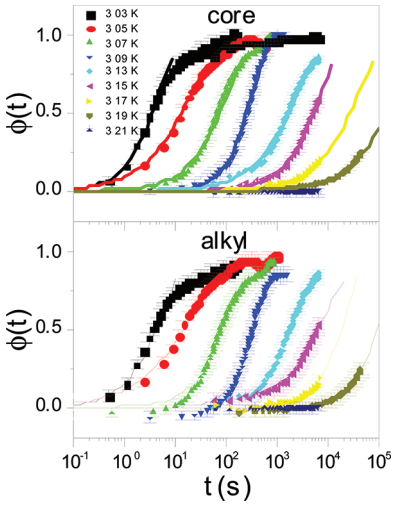

Figure 6. Crystallization kinetics at different temperatures, obtained by fitting (a) the aromatic C−H absorption bands (Figure 2e) and (b) the alkyl absorption bands (Figure 2c) with eq 2. The crystallization rate varies by orders of magnitude within a small temperature range. The lines are fits with the Avrami equation (eq 3).

Figure 2. In the analysis of kinetics different spectra from the quasi-static measurements are selected as reference phase profiles for eq 2, with time as the independent variable. The C_r profile is obtained from the heating run at the respective jump temperature. The Col_h profile is obtained from the cooling run spectra for jump temperatures above 315 K, where kinetics is slow. For the remaining temperatures, the first temperature recorded after the jump is used. This way, the approximations made for the quasi-static case are avoided and comparison between aromatic and alkyl moieties is direct. The increase of the volume fraction corresponding to the C_r phase following jumps from the Col_h phase at 363 K to different temperatures is shown in Figure 6. The volume fraction is compared for two bands; the aromatic C−H and the alkyl C−H absorption bands. Both show the characteristic sigmoidal increase with time. The results are fitted with the modified Avrami equation,[37]

$$\phi(t) = \phi_0 + (\phi_\infty - \phi_0)(1 - \exp(-\ln 2(t/t_{1/2})^n)) \quad (3)$$

where $\phi_0 = 0$, $\phi_\infty = 1$ are crystallinity values at $t = 0, \infty$, respectively, $t_{1/2}$ is the characteristic crystallization time and n the Avrami exponent. The Avrami equation describes well the data, up to volume fractions of ~0.8 and the value of the exponent n is about 1 signifying first order kinetics. In addition, the kinetics of the aromatic C−H and the alkyl C−H vibrations are nearly indistinguishable at all temperatures investigated. This suggests that formation of the C_r phase is not driven solely by the alkyl chains and this despite their changing conformations on approaching the C_r phase from higher temperatures (Figure 5). We will return to this point after discussing the DS and rheology kinetics.

The kinetics of phase transformation was studied subsequently with DS. The $\varepsilon^*(\omega)$ of DLCs is dominated by the dipolar dynamics of the C−Br group as indicated in Figure 7. The main relaxation mechanism within the Col_h phase corresponds to the disk axial motion,[15,38−41] whereas within the C_r phase, the latter mechanism is practically frozen (as shown earlier by independent solid state NMR measurements).[16] The figure displays the evolution of the dielectric loss following a temperature jump

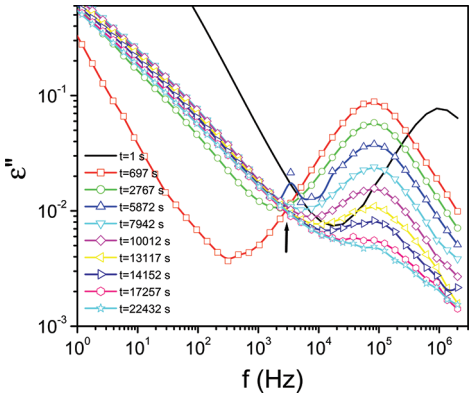

Figure 7. Time-dependence of the dielectric loss following a temperature jump from 373 to 315 K. The solid line (t = 1 s) is the spectrum taken at the initial temperature (373 K), whereas all other curves were taken under isothermal conditions (315 K) at the indicated times. The vertical arrow signifies an isosbestic point.

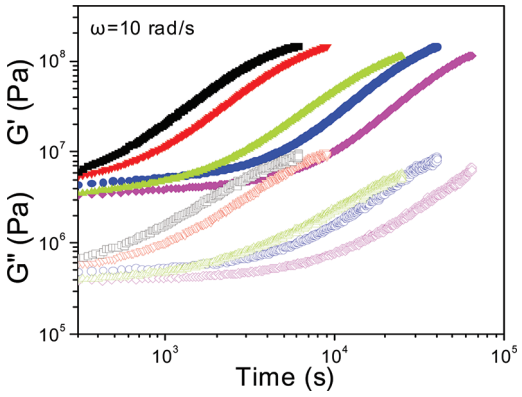

Figure 9. Time-dependence of the storage (filled symbols) and loss (open symbols) moduli following temperature jumps from the same initial temperature (373 K) to different final temperatures: (squares), 315 K; (down triangles), 316 K; (up triangles), 318 K; (circles), 319 K; and (rhombi), 320 K.

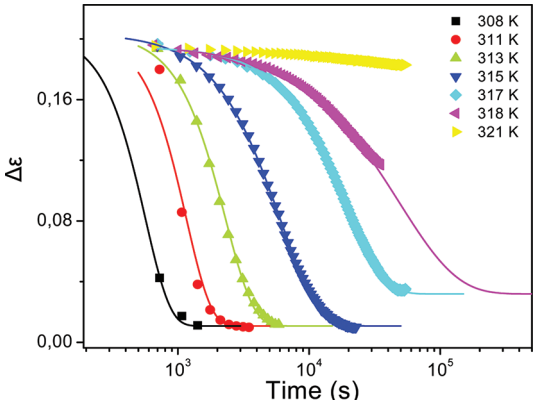

Figure 8. Time-dependence of the dielectric strength following consecutive temperature jumps from 373 K to different final temperatures corresponding to the following: (squares), 308 K; (circles), 311 K; (up triangles), 313 K; (down triangles), 315 K; (rhombi), 317 K; (left triangles), 318 K; and (right triangles), 321 K. The lines are fits to eq 3.

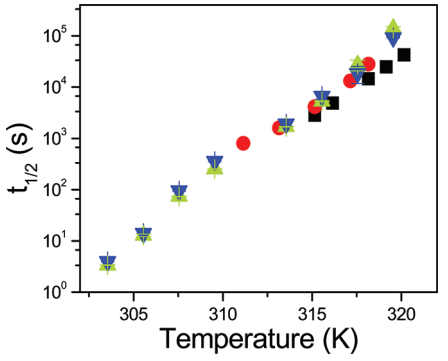

Figure 10. Half-times of the Col_h to C_r phase transformation plotted as a function of temperature, obtained from different techniques by fitting the volume fractions of the C_r phase to the Avrami equation (eq 3): (black squares), rheology; (red circles), α-process intensity from DS; (green up triangles), C−H out-of-plane IR bands (Figure 2e); and (blue down triangles), alkyl chain IR bands (Figure 2c).

from 373 K to different final temperatures favoring the C_r phase. It can be seen that during the transformation, the intensity of the mechanism corresponding to the disk axial motion is reduced at the expense of a slower contribution thus giving rise to an isosbestic point at about 3×10^3 Hz. The spectra were analyzed using a summation of two HN modes and the time-dependence of the dielectric strength corresponding to the "fast" process associated with the freezing of the disk axial motion is depicted in Figure 8 for the different final temperatures. It can be seen that for a quench to 321 K, initiation of the transformation requires more than a day. To extract the characteristic transformation time, the Avrami equation was employed and the results are discussed below.

Rheology is also a very sensitive probe of the phase transformation since the two phases possess drastically different viscoelastic properties (Figure 1).[21] Figure 9 depicts the time-dependence of the storage (G') and loss (G'') moduli following a temperature jump from 373 K to different final temperatures within the C_r phase. In all cases, the characteristic S-shape increase of the moduli is seen reflecting the transformation from an undercooled (viscoelastic) Col_h phase to the final (elastic) C_r phase. The volume fraction of the final C_r phase was obtained through suitable models of composites (using the "parallel" and "series" models) as described elsewhere in detail.[21]

The characteristic kinetic times obtained by IR spectroscopy are compared with the results from rheology and dielectric spectroscopy in Figure 10. The figure shows characteristic times of the Col_h to C_r phase transformation within 17 K spanning a time-range from 1s to 1 day. To a good approximation, the different probes share similar kinetics. The fact that the characteristic times become longer with increasing temperature is suggestive of a nucleation and growth process. IR spectroscopy offers the advantage of much higher time resolution and is practically limited only by the cooling rate of the heating stage. In addition, it is shown that crystallization rates and Avrami exponents for the aromatic core and the alkyl chains are equal, within measurement uncertainty. The Avrami exponent values by IR spectroscopy ($n \approx 1$, i.e., first order kinetics) are, however, lower than the ones obtained by both DS and rheology (Supporting Information, Figure S4).

dx.doi.org/10.1021/jp207410f |J. Phys. Chem. B 2011, 115, 14919–14927

According to a nucleation and growth process, the characteristic times are a function of the final "crystallization" temperature as $t_{1/2} = \tau_0 \exp(B/(T - T_0))\exp(-\Delta G^*/k_B T)$, where τ_0 is a constant. The first exponential term refers to the transport term and has the usual Vogel−Fulcher−Tammann dependence that is obtained from T-dependent DS measurements ($\tau_0 = 5.0 \times 10^{-10}$s, $B = 1700$ K, $T_0 = 146$ K).[19] The second one refers to the nucleation barrier, ΔG^*, giving the Gibbs free energy required for the formation of the new phase. Typically, the latter is obtained by plotting $\ln\tau_{1/2} - \ln\tau_0^* - B/(T - T_0)$ vs $1/T$ and amounts to 4.8 ± 0.3 eV in DS and to 5.2 ± 0.1 and 5.6 ± 0.2 eV in rheology and IR, respectively. This again shows that the different techniques are probing the same phase transformation.

4. CONCLUSIONS

The details of the phase transformation from the high temperature liquid crystalline phase to the crystalline phase were studied in a monobromo hexa-*peri*-hexabenzocoronene derivative by following changes in the infrared absorption spectra. These were complemented by independent structural, thermodynamic, and dynamic techniques that unambiguously provide the phase characteristics. Vibration modes corresponding to both the alkyl chain and to the aromatic core have been employed as fingerprints of the phase state and allowed, for the first time, a study of the phase transformation dynamics by separate probing of the alkyl chains and of the core.

Among the different vibration modes, the C−H out-of-plane bending gives a clear signature of the phase transformation. In addition, the alkyl chain conformations are also a sensitive probe of the phase change with roughly 2/3 and 1/3 of the conformations being gauche in the liquid crystalline and crystalline states, respectively. With IR, the kinetics of the formation of the crystalline phase was followed over an extraordinarily broad time-window ($1-10^5$ s) within only 17 K and found to comply with a nucleation and growth process in agreement with independent probing of the kinetics via dielectric and viscoelastic means. The identical kinetic times of transformation extracted from the alkyl chains and aromatic cores suggest that the packing of both the cores and the alkyl chains that drive the phase transformation from the undercooled liquid crystalline to the crystalline herringbone structure.

■ ASSOCIATED CONTENT

Supporting Information. Pressure−volume−temperature measurements used to obtain the equation of state, macroscopic Grüneisen parameter, Avrami exponents from the different kinetic experiments and wide-angle X-ray scattering 1D integrations. This material is available free of charge via the Internet at http://pubs.acs.org.

■ AUTHOR INFORMATION

Corresponding Author

*Tel: +30-2651-008564; Fax: +30-2651-008693. E-mail: gfloudas@cc.uoi.gr (G.F.), papadopoulos@mpip-mainz.mpg.de (P.P.).

■ ACKNOWLEDGMENT

The research Project is co-funded by the European Union-European Social Fund (ESF) & National Sources, in the framework of the program "HRAKLEITOS II" of the "Operational Program Education and Life Long Learning" of the Hellenic Ministry of Education, Life Long Learning and religious affairs. The current work was supported by the Research unit on Dynamics and Thermodynamics of the UoI financed by ESPA 2007-2013 (call 18). We thank A. Best, A. Hanewald, M. Bach (MPI-P), and G. Tsoumanis (UoI) for technical support. Financial support of the Deutsche Forschungsgemeinschaft, SFB 625 is gratefully acknowledged.

■ REFERENCES

(1) *Handbook of Liquid Crystals*; Demus, D., Goodby, J., Gray, G. W., Spiess, H.-W., Vill, V., Eds.; Wiley-VCH: Weinheim, 1998.
(2) Wu, J.; Pisula, W.; Müllen, K. *Chem. Rev.* **2007**, *107*, 718–747.
(3) Schmidt-Mende, L.; Fechtenkötter, A.; Müllen, K.; Moons, E.; Friend, R. H.; MacKenzie, J. D. *Science* **2001**, *293*, 1119–1122.
(4) Ito, S.; Wehmeier, M.; Brand, J. D.; Kübel; Epsch, R.; Rabe, J. P.; Müllen, K. *Chem.—Eur. J.* **2006**, *6*, 4327–4342.
(5) Fischbach, I.; Pakula, T.; Minkin, P.; Fechtenkötter, A.; Müllen, K.; Spiess, H. W. *J. Phys. Chem. B* **2002**, *106*, 6408–6418.
(6) Ochsenfeld, C.; Brown, S.; Schnell, I.; Gauss, J.; Spiess, H. W. *J. Am. Chem. Soc.* **2001**, *123*, 2597–2606.
(7) de Gennes, P. G. *J. Phys., Lett.* **1983**, *44*, 1.
(8) Tasios, N.; Grigoriadis, C.; Hansen, M. R.; Wonneberger, H.; Li, C.; Spiess, H. W.; Müllen, K.; Floudas, G. *J. Am. Chem. Soc.* **2010**, *132*, 7878.
(9) Glüsen, B.; Kettner, A.; Kopitzke, J.; Wendorff, J. H. *J. Non-Cryst. Solids* **1998**, *241*, 113.
(10) Möller, M.; Wendorff, J. H.; Werth, M.; Spiess, H. W. *J. Non-Cryst. Solids* **1994**, *170*, 295–299.
(11) Grigoriadis, C.; Haase, N.; Butt, H.-J.; Müllen, K.; Floudas, G. *Adv. Mater.* **2010**, *22*, 1403–1406.
(12) Leisen, J.; Werth, M.; Boeffel, C.; Spiess, H. W. *J. Chem. Phys.* **1992**, *97*, 3749.
(13) Vallerien, S. U.; Werth, M.; Kremer, F.; Spiess, H. W. *Liq. Cryst.* **1990**, *8*, 889.
(14) Elmahdy, M. M.; Floudas, G.; Kastler, M.; Müllen, K. *J. Phys. C* **2008**, *20*, 244105.
(15) Elmahdy, M. M.; Floudas, G.; Mondeshki, M.; Spiess, H. W.; Dou, X.; Müllen, K. *Phys. Rev. Lett.* **2008**, *100*, 107801–107804.
(16) Elmahdy, M. M.; Dou, X.; Mondeshki, M.; Floudas, G.; Butt, H.-J.; Spiess, H. W.; Müllen, K. *J. Am. Chem. Soc.* **2008**, *130*, 5311–5319.
(17) Feng, X.; Marcon, V.; Pisula, W.; Hansen, M. R.; Kirkpatrick, J.; Grozema, F.; Andrienko, D.; Kremer, K.; Müllen, K. *Nat. Mater.* **2009**, *8*, 421–426.
(18) van de Craats, A. M.; Warman, J. M.; Fechtenkötter, A.; Brand, J. D.; Harbison, M. A.; Müllen, K. *Adv. Mater.* **1999**, *11*, 1469.
(19) Haase, N.; Grigoriadis, C.; Butt, H.-J.; Müllen, K.; Floudas, G. *J. Phys. Chem. B* **2011**, *115*, 5807.
(20) Elmahdy, M. M.; Mondeshki, M.; Dou, X.; Butt, H.-J.; Spiess, H. W.; Müllen, K.; Floudas, G. *J. Chem. Phys.* **2009**, *131*, 114704–9.
(21) Grigoriadis, C.; Haase, N.; Butt, H.-J.; Müllen, K.; Floudas, G. *Soft Matter* **2011**, *7*, 4680.
(22) Carminati, M.; Brambilla, L.; Zerbi, G.; Muellen, K.; Wu, J. *J. Chem. Phys.* **2005**, *123*, 144706.
(23) Marcon, V.; Vehoff, T.; Kirkpatrick, J.; Jeong, C.; Yoon, D. Y.; Kremer, K.; Andrienko, D. J. *J. Chem. Phys.* **2008**, *129*, 094505.
(24) *Broadband Dielectric Spectroscopy*; Kremer, F., Schönhals, A., Eds.; Springer: Berlin, 2002.
(25) Floudas, G. *Prog. Polym. Sci.* **2004**, *29*, 1143.
(26) Sujeewa, D.; Silva, M.; de, Zeng, X.-B.; Ungar, G.; Spells, S. J. *Macromolecules* **2002**, *35*, 7730.
(27) Singh, S.; Wegmann, J.; Albert, K.; Müller, K. *J. Phys. Chem. B* **2002**, *106*, 878.
(28) Maroncelli, M.; Qi, S. P.; Strauss, H. L.; Snyder, R. G. *J. Am. Chem. Soc.* **1982**, *104*, 6237.
(29) Senak, L.; Davies, M. A.; Mendelsohn, R. *J. Phys. Chem.* **1991**, *95*, 2565–2571.

(30) Tashiro, K.; Sasaki, S.; Kobayashi, M. *Macromolecules* **1996**, *29*, 7460.
(31) Tashiro, K.; Sasaki, S.; Gose, N.; Kobayashi, M. *Polymer J* **1998**, *30*, 485.
(32) Socrates, G. *Infrared and Raman Characteristic Group Frequencies. Tables and Charts*; John Wiley & Sons Ltd: New York, 2001.
(33) Bauschlicher, C. W.; Bakes, E. L. O. *Chem. Phys.* **2000**, *262*, 285.
(34) Snyder, R. G. *J. Chem. Phys.* **1967**, *47*, 1316.
(35) Hagemam, H.; Snyder, R. G.; Peacock, A. J.; Mandelkern, L. *Macromolecules* **1989**, *22*, 3600.
(36) McKean, J. M. *Chem. Soc. Rev.* **1978**, *7*, 399.
(37) Avrami, M. J. *J. Chem. Phys.* **1939**, *7*, 1103. **1940**, *8*, 212. **1941**, *9*, 177.
(38) Ngai, K. L. *J. Non-Cryst. Solids* **1996**, *197*, 1–7.
(39) Groothues, H.; Kremer, F.; Collard, D. M.; Lillya, C. P. *Liq. Cryst.* **1995**, *18*, 117–121.
(40) Möller, M.; Wendorff, J. H.; Werth, M.; Spiess, H. W.; Bengs, H.; Karthaus, O.; Ringsdorf, H. *Liq. Cryst.* **1994**, *17*, 381–395.
(41) Kruglova, O.; Mendes, E.; Yildirim, Z.; Wübbenhorst, M.; Mulder, F. M.; Stride, J. A.; Picken, S. J.; Kearley, G. J. *Chem. Phys. Chem.* **2007**, *8*, 1338–1344.